Appendix

Table of contents

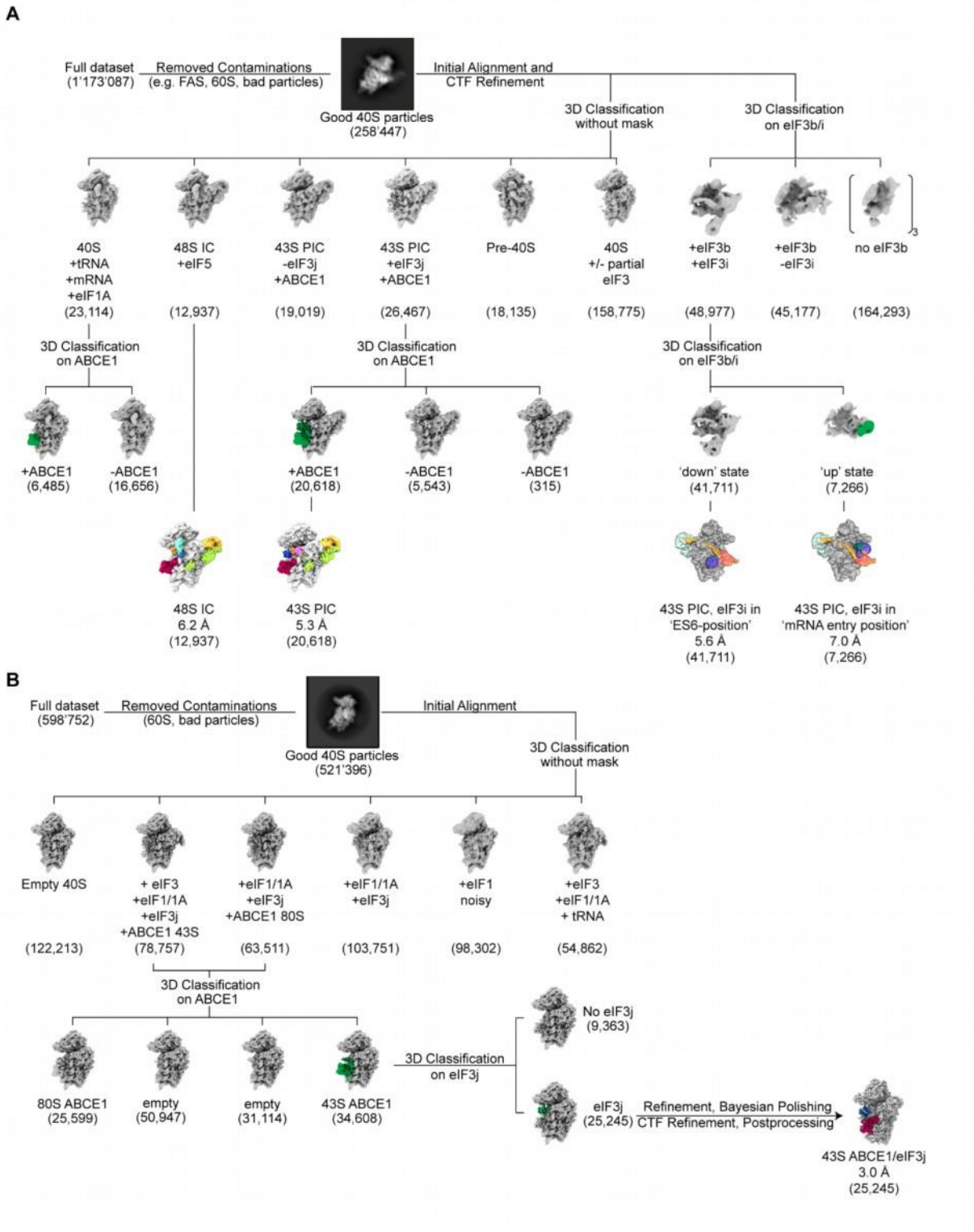

Appendix Figure S1 - Sorting scheme for the yeast native 40S sample and the 43S-PIC-XL sample.

A After 2D classification of the full dataset, approximately 260.000 particles representing 40S subunits were selected. By 3D classification into six classes, 29% of the particles were unambiguously identified as pre-initiation complexes, amongst them a 43S PIC class containing eIF1, eIF1A, eIF3 and ABCE1 with stably bound eIF3j and one class representing a partial 48S initiation complex containing eIF1A, eIF3, eIF5, the TC, and ABCE1. The 48S IC was refined to 6.2 Å and the eIF3j-containing 43S was sub-classified for ABCE1, yielding a 5.3 Å

reconstruction of the 43S PIC. In total, 62% of the found initiation-factor-containing 40S particles contained ABCE1 after focused classification for ABCE1 presence. Independently, focused classification on the particles containing the eIF3b/i/g module was performed to assess conformational distribution of eIF3i/g with respect to eIF3b. 85% of the particles contained eIF3i in the "ES6-position", while in 15% of particles, eIF3i was in the "mRNA entry-position".

B After 2D classification of the full dataset, 521,396 particles representing 40S subunits were selected. By 3D classification into six classes, two classes containing ABCE1 were identified. These were subclassified by sequentially using a mask on the ABCE1 region as well as a mask on eIF3j, in order to identify one class containing both eIF3j and ABCE1 in the semi-open conformation as observed in the native sample. This class represents 4.8% of the total dataset and was refined to 3.0 Å.

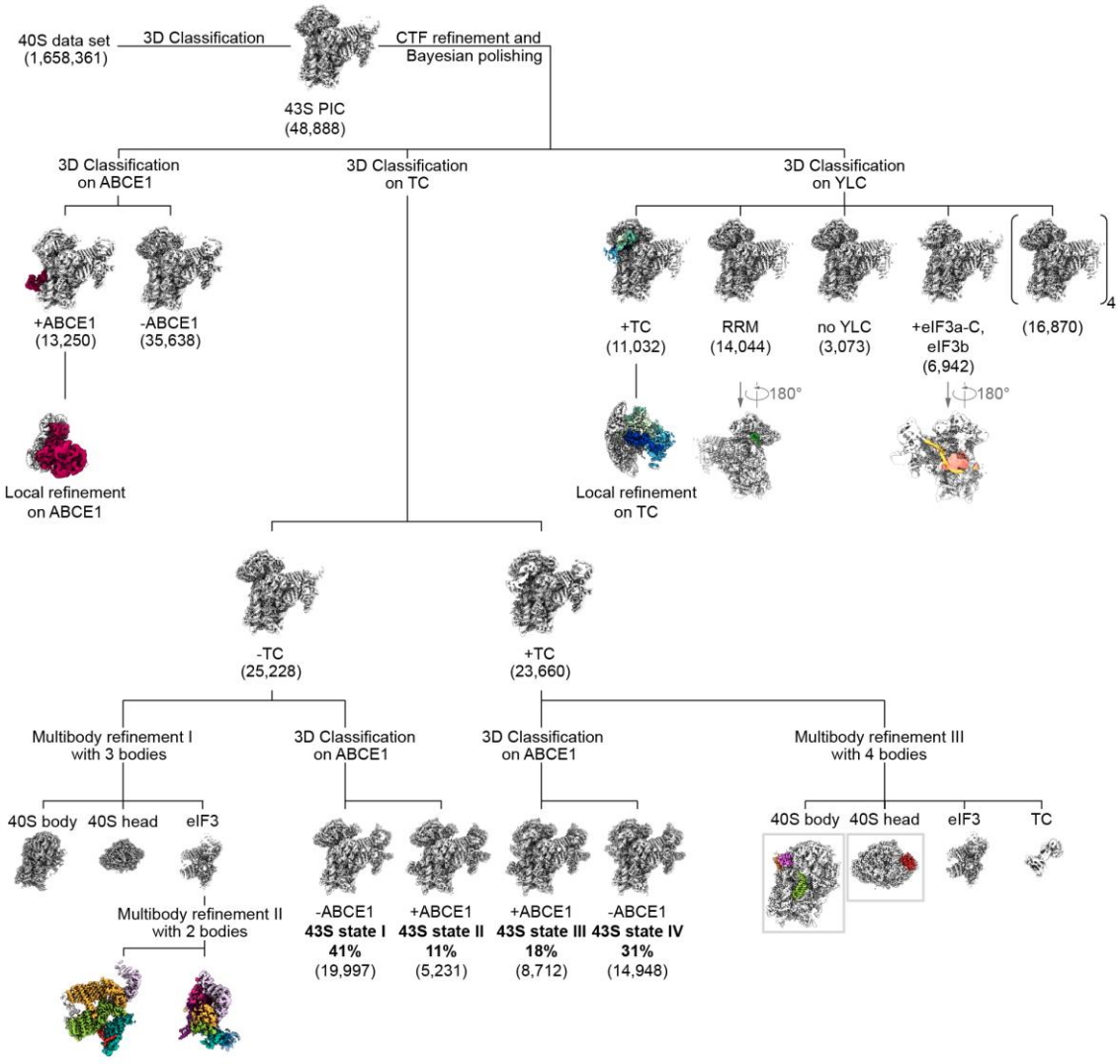

Appendix Figure S2 - Sorting scheme for the human native small 40S sample.

The data set was first classified for presence of initiation factors (see Materials and Methods). 2.9% of all particles contained the eIF3 PCI-MPN core at the back side of the 40S and partial densities for the YLC at the mRNA entry site, the TC in the ISS, and ABCE1. Focused classifications were performed using a binary mask with soft edges

to obtain homogenous populations of 43S complexes. Focused classification on the TC yielded two classes with and without the TC that also differed in the conformation of the 40S head (closed latch without TC and P_{OUT} state). These two classes were sub-classified focusing on ABCE1, yielding the four main classes shown in Fig. 2. To obtain the highest possible resolution, we independently performed multi-body refinements on TC-bound and -unbound classes. The TC-lacking class containing the eIF3-PCI-MPN core was refined in two steps: first, the 43S was divided into three bodies (40S body, 40S head and eIF3; multi-body refinement I). Then the body containing the eIF3-PCI-MPN core was re-centered, the 40S SSU signal subtracted and a multi-body refinement with two bodies was performed (multi-body refinement II) that were used for model building. Particles containing the TC were subjected to multi-body refinement III with four bodies (40S body and head, eIF3-PCI-MPN core and TC) yielding well-resolved densities for the eIF3c-NTD on the body and eIF3d on the head used for model building. Classification of the entire 43S data set focusing on ABCE1 followed by focused refinement yielded a well-resolved map from 27% ABCE1-containing particles used for model building. Focused classification on the YLC revealed various compositional and conformational states. One class represented a very stable complete 43S complex in P_{OUT} state and focused refinement yielded a well-resolved map of the TC used for model building. A focused refinement resulted in the best resolved map for the TC, which could be used for model building; two other classes were enriched in stably bound YLC, one showing the clear connection between the PCI-MPN core and the YLC and one with a well-resolved density for a RRM adjacent to the mRNA entry site and density in the mRNA channel.

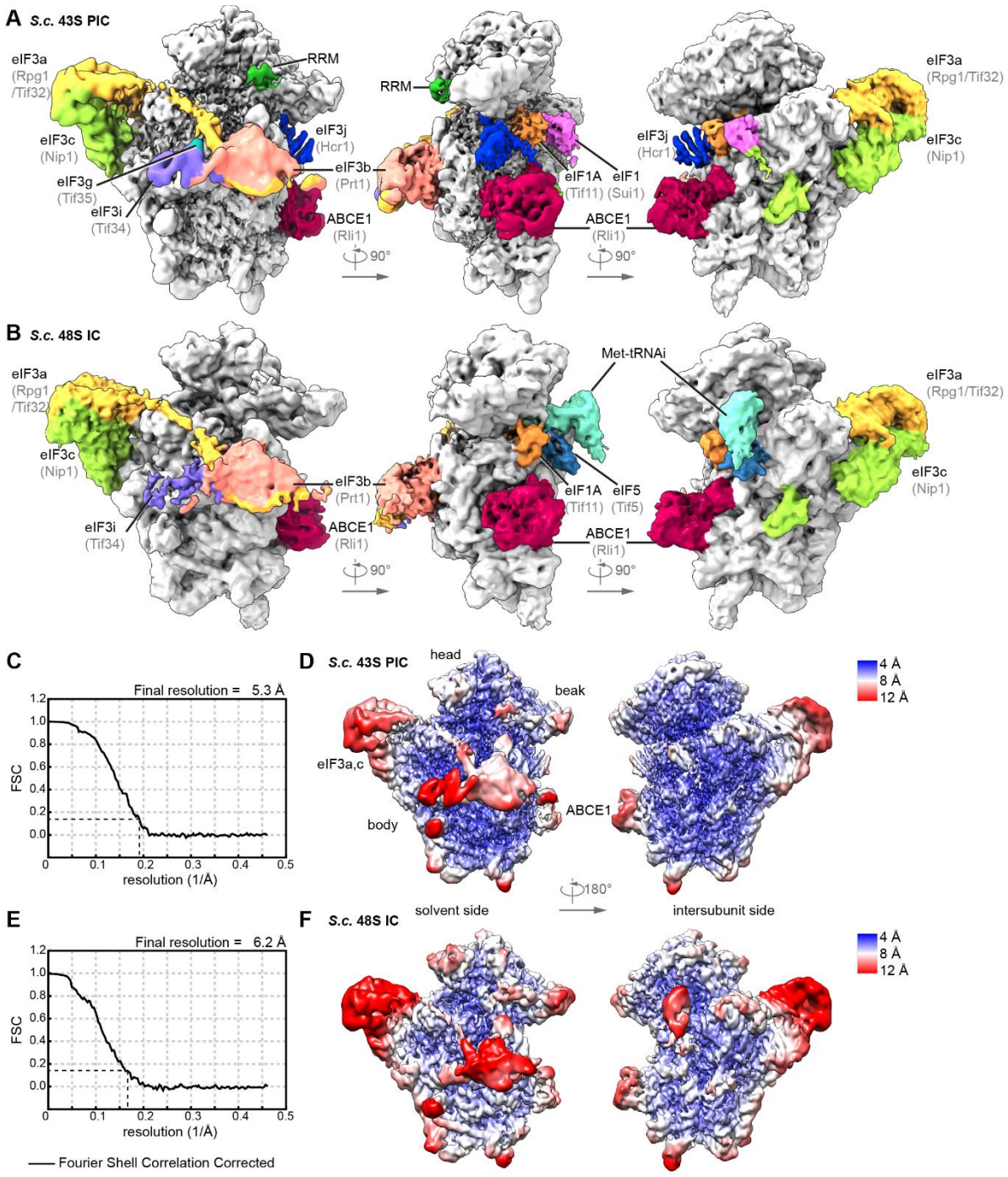

Appendix Figure S3 - Overview and resolution of the yeast 43S PIC and 48S IC.

A, B Three views on the 3D reconstructions of the yeast 43S PIC (A) and the 48S IC (B) low-pass filtered according to local resolution.

C, D Gold standard Fourier Shell Correlation (FSC) curve (C) and 3D reconstruction the yeast 43S PIC colored and filtered according to local resolution (D).

E, F Gold standard Fourier Shell Correlation (FSC) curve (E) and 3D reconstruction the yeast 48S IC colored and low-pass filtered according to local resolution (F).

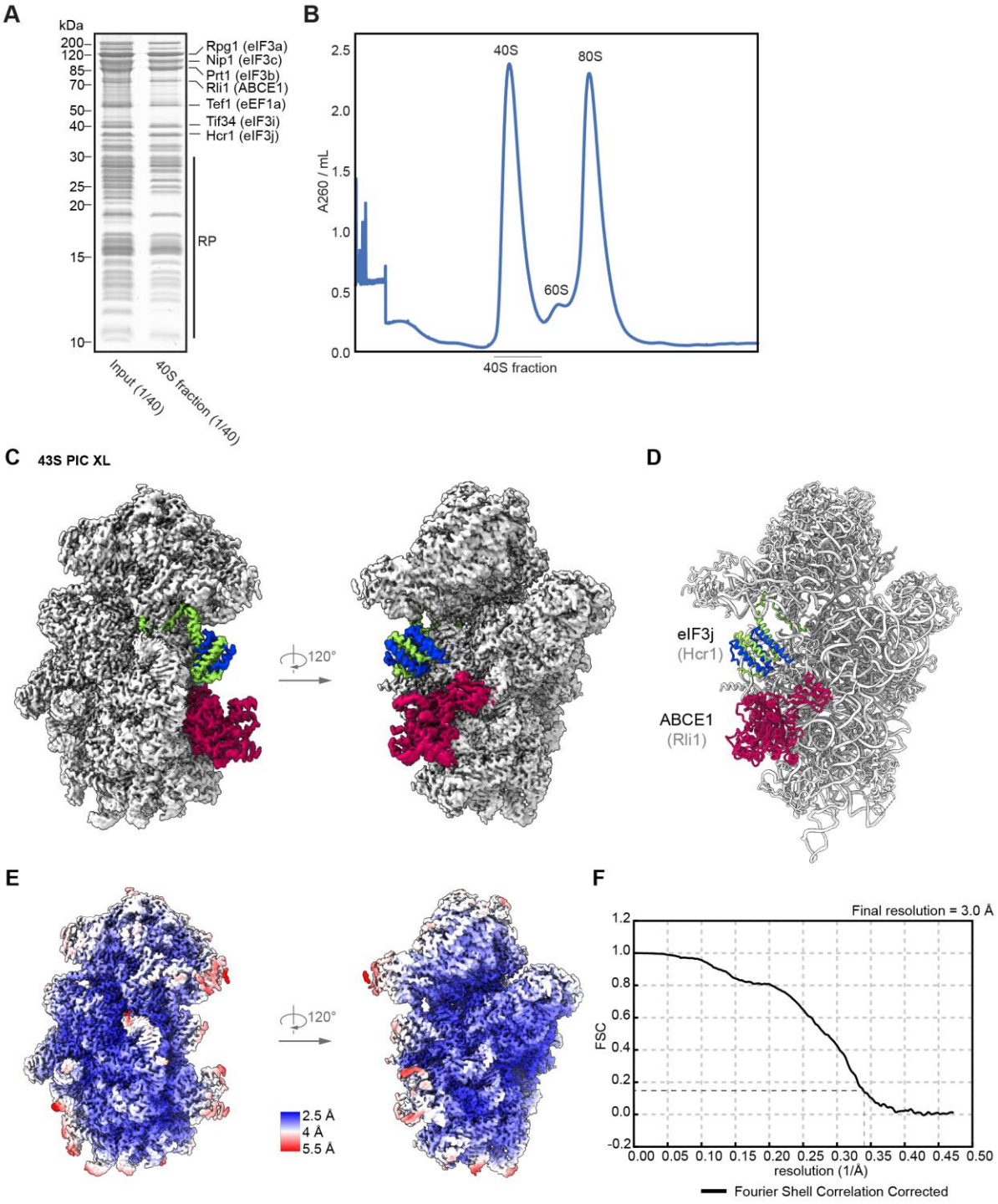

Appendix Figure S4 - Sample preparation and cryo-EM structure of the yeast 43S PIC-XL.

A SDS-PAGE gel of the Nip1-TAP pullout sample before and after sucrose gradient purification.

B UV profile from Nip1-TAP pullout elution fraction separated on a sucrose gradient (10–50%) by ultracentrifugation.

C Two views of the 3D reconstruction of the yeast 43S PIC-XL, low-pass filtered at local resolution.

D Atomic model of the yeast 43S PIC-XL.

E, F 3D reconstruction the yeast 43S PIC-XL colored and low-pass filtered according to local resolution (E) and gold standard Fourier Shell Correlation (FSC) curve (F).

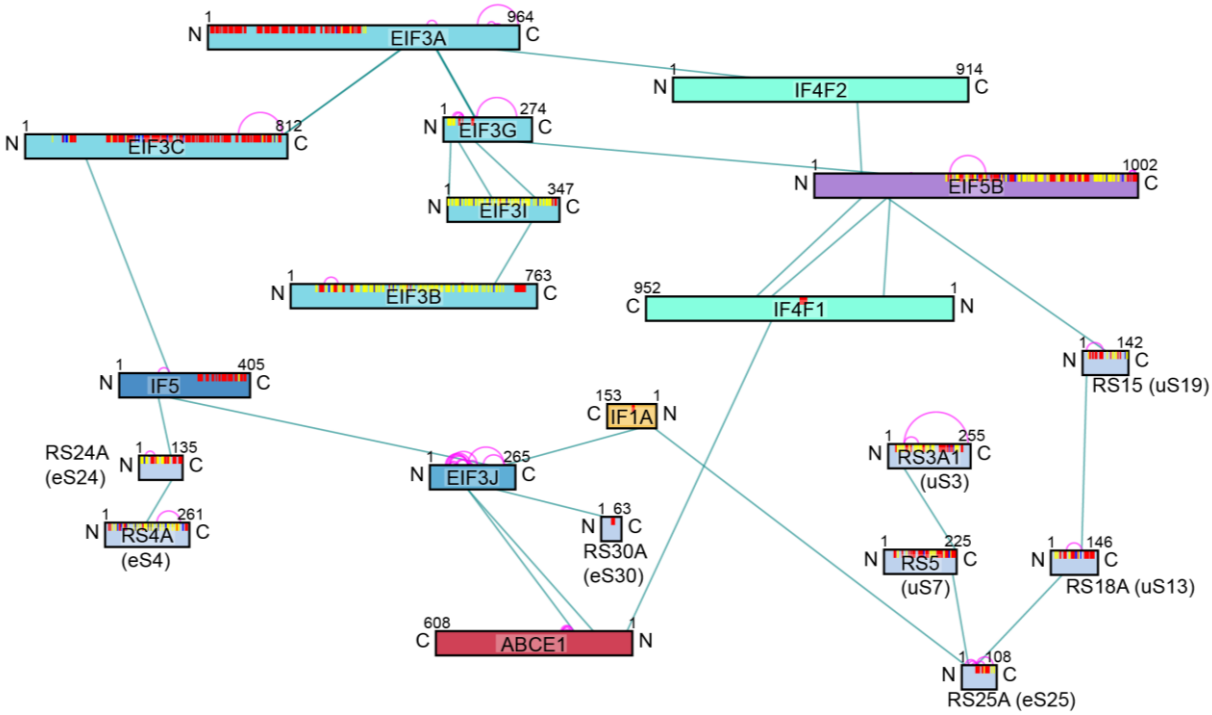

Appendix Figure S5 - Crosslink derived connectivity network of the yeast ABCE1 43S PIC.

ABCE1-43S pre-initiation complex was affinity-purified from yeast cell extracts using TAP-tagged Nip1 (eIF3c) protein. Schematic representation of the obtained 43 inter-protein and 74 intra-protein crosslinks (Appendix Table 3) with a focus on initiation factors and ABCE1. Proteins are represented as bars with subunits and secondary structures indicated according to UniProt color scheme. The lengths of protein and crosslinks are scaled to the amino acid sequence.

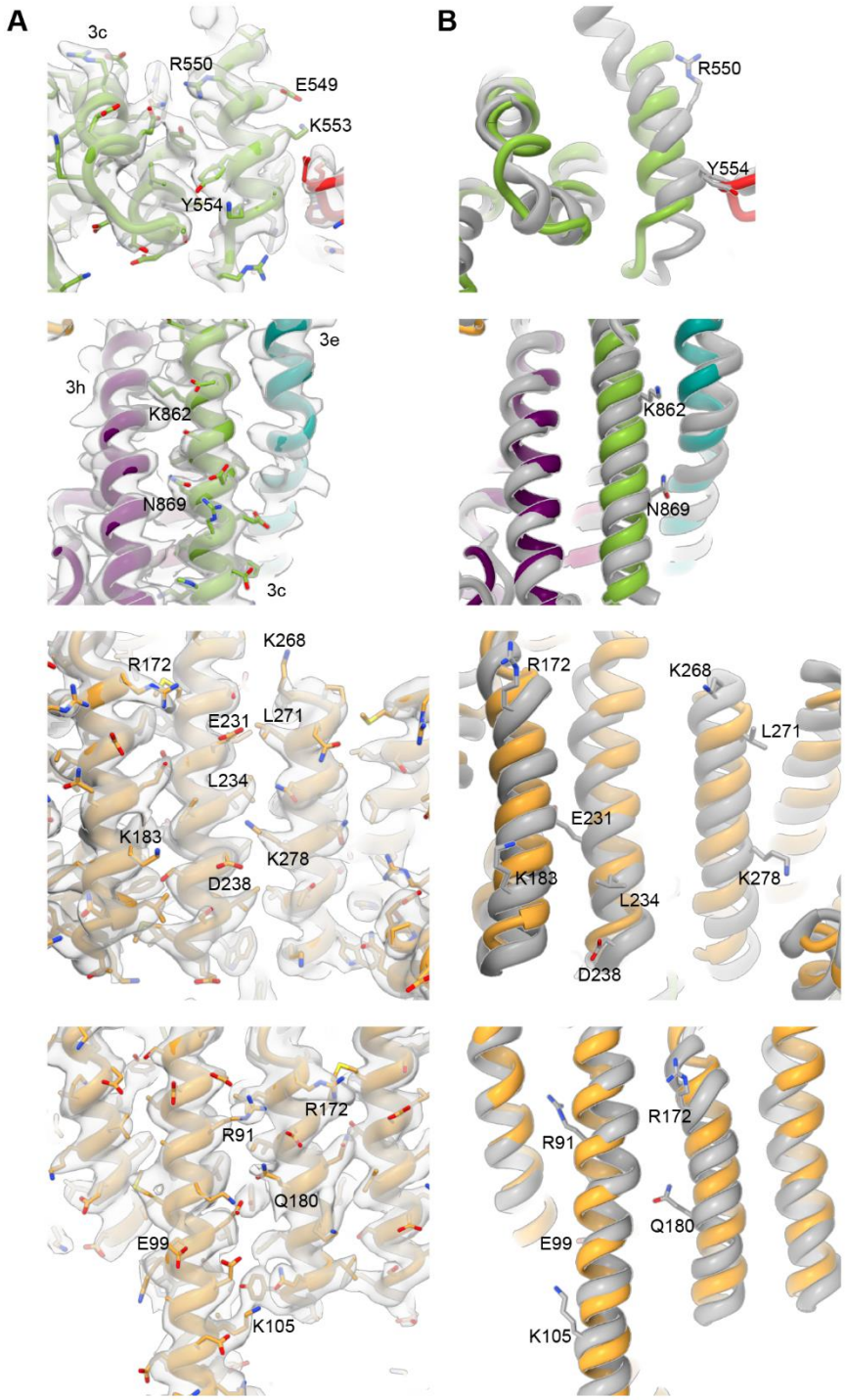

Appendix Figure S6 - Corrected register shifts in the helices of the PCI-MPN core in the human 43S PIC.

A Selected sites of the PCI-MPN core shown with cryo-EM density

B Comparison of the new model and the starting model (PDB 5A5T, des Georges *et al.*, 2015) coloured in grey. Same view and colours as in (A). Side chains are labelled to highlight the register shifts.

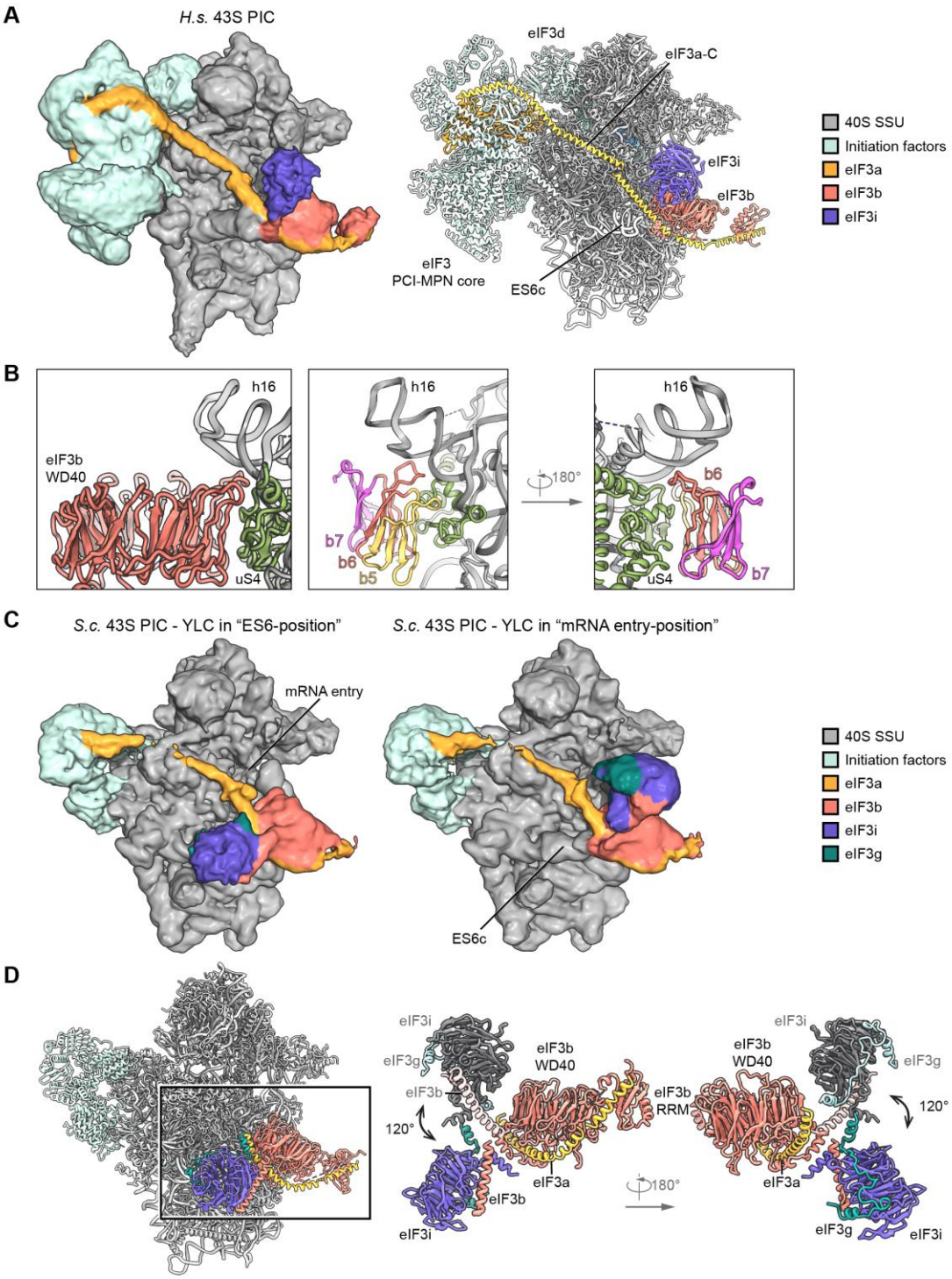

Appendix Figure S7- Position of the eIF3 YLC and the eIF3a-CTD in yeast and human 43S PICs.

A Cryo-EM map of the human 43S PIC class obtained after local classification on the YLC (see Appendix Fig S2), low-pass filtered at 6 Å (left). Composite model of the human 43S PIC as in Fig. 2 (right). The view focuses on the mRNA entry side of the 40S, showing the YLC and the rod-like eIF3a density representing its C-terminus spanning from the back side of the 40S to the YLC.

B Interactions of eIF3b with the ribosome; models for eIF3g and eIF3a not shown. Two different views show only WD40 blades (b) 5 to 7 of eIF3b. In β-strand D5 (nomenclature refers to Liu *et al*, 2014) Arg505, Arg507 and

Leu509 and in β-strand D6 Val558, Glu560 are facing towards uS4. The loop between B5-C5 (485-490) interacts with the rRNA backbone of the h16-h17 junction and uS4 (Tyr 165) and the loop between D5 and A6 (especially Phe510) interacts with Lys121 of uS4. h16 is contacted *via* the loop B6-C6 (res 532-541) *via* backbone interactions.

C Two different states of the yeast YLC obtained after focused classification. In one state ("ES6-position") the eIF3g-eIF3i module bound to the eIF3b most C-terminal helix is facing towards expansion segment ES6c, in the other state ("mRNA entry-position") it faces towards the mRNA entry, similar as in the human 43S PIC and as described previously (Erzberger *et al.*, 2014; Llacer *et al.*, 2018). 85% of the particles contained eIF3i in the ES6-position and 15% of particles in the mRNA entry-position (see Appendix Fig S1).

D Molecular model of the yeast 43S PIC with the YLC in (left) and overlay of the two positions. In the overlay the mRNA entry-position eIF3i is colored grey and eIF3g light blue and the eIF3b C-terminal helix white. The loop between the two most C-terminal helices of the eIF3b CTD (Thr697-Asp701) serves as a hinge for rotation.

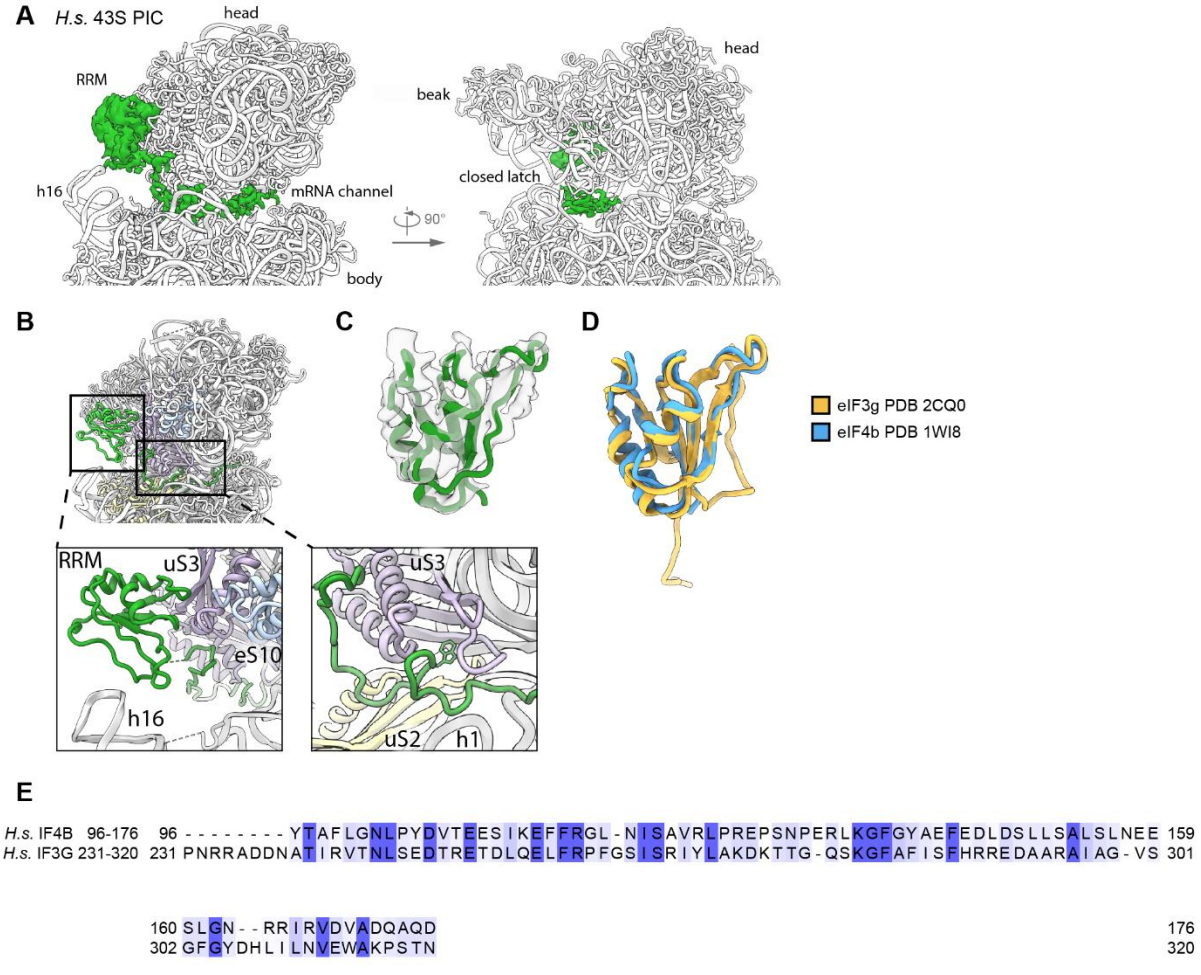

Appendix Figure S8 - Position of the eIF3g or eIF4b RRM and density in the mRNA channel.

A Zoomed views on the mRNA channel as viewed from the ISS focusing on an extra density (green) on top of rRNA h16 and inside the mRNA channel. The isolated density is low-pass filtered according to local resolution.

B Overview and zoomed views on the poly-alanine model for an RRM on top of h16 and for the density in the mRNA channel in context of the 43S PIC. Interacting r-proteins and rRNA and the clearly visible tryptophan residue interacting with uS3 in the mRNA entry channel are highlighted.

C Model for a typical RRM-fold fitted into the corresponding isolated density.

D Overlay of the RRMs of eIF4b and eIF3g.

E Sequence alignment of the RRM of human eIF4b and eIF3g, which shows 21.7/55.4% sequence identity/similarity.

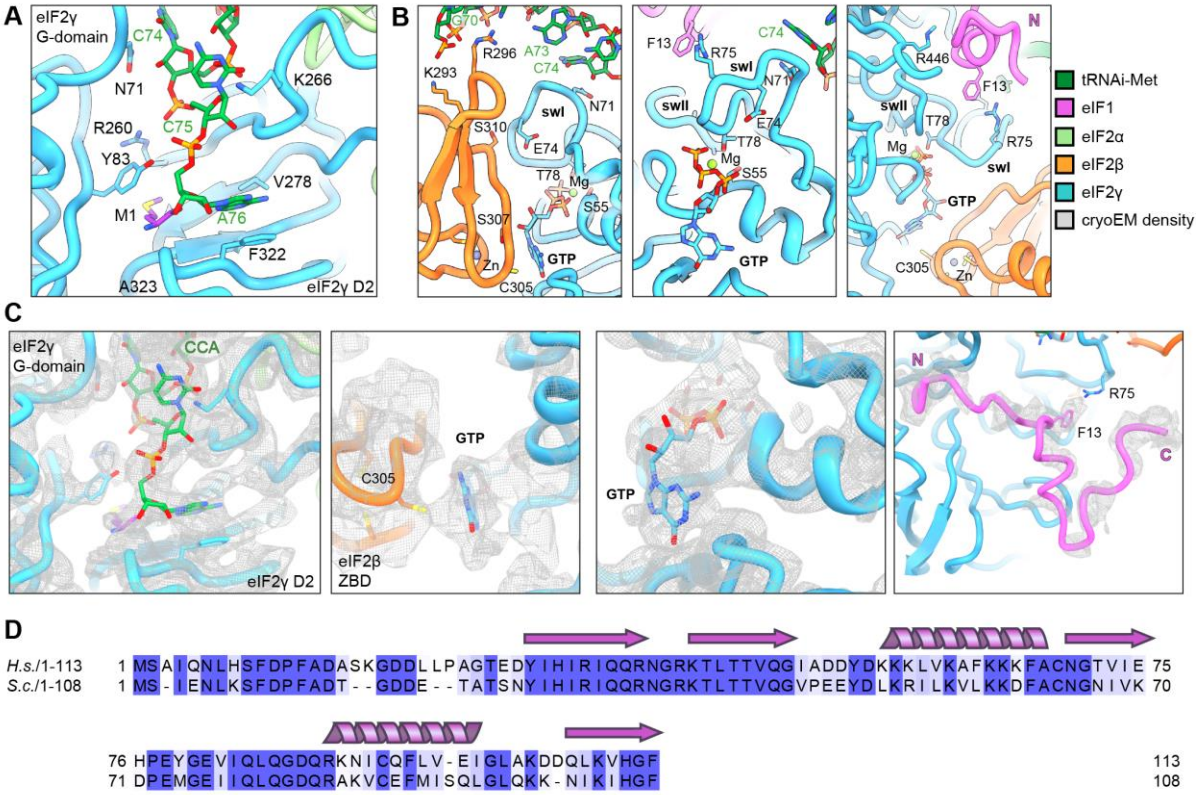

Appendix Figure S9 - Molecular interactions of the TC in the complete human 43S PIC.

A, B View focusing on the interactions of methionylated $tRNA_i$ with eIF2γ (A), the ZBD of eIF2β packing upon the nucleotide binding pocket of eIF2γ (B) as shown in Figure 7. Binding to $tRNA_i$ (left) and the switch loops (sw) of eIF2γ contacting the *de novo* built eIF1 N-terminal tail (middle and right).

C Zoomed views of fits of the TC model into the cryo-EM map. Highlighted are the CCA-end of $tRNA_i$ bound to eIF2γ, the guanine base lock-up by the eIF2β ZBD, the GTP in the eIF2γ nucleotide binding pocket and the *de novo* built N-terminal tail (res 4-30) of eIF1.

D Sequence alignment between the yeast and human eIF1 shows a sequence identity of 61.1% and a sequence similarity of 87.0% (N-terminus of eIF1 (4-30) shows 55.6/74.1% sequence identity/similarity) indicating a high degree of conservation.

Appendix Table S1 - Data collection, refinement, and model composition of the yeast initiation complexes.

	***S.c.* 43S PIC PDB 6ZCE EMDB 11160**	***S.c.* 48S IC PDB 6ZU9 EMDB 11439**	***S.c.* 43S PIC-XL PDB 7A1G EMDB 11608**
Data collection			
Voltage (kV)	300		
Electron exposure (e–/Å^2)	25		44.8
Defocus range (μm)	−1.1 to −2.3		−0.5 to −2.5
Pixel size (Å)	1.084		1.059
Symmetry imposed	C1		
Refinement			
Particle images (no.)	20,618	12,937	25,245
Map resolution (Å)	5.3	6.2	3.0
FSC threshold	0.143		
Map sharpening B factor (Å^2)	-48.5	-100	-24
Model composition			
Correlation coefficient (%; Phenix)	64	60	82
Models used (PDB codes)	5NDG, 6FYY, 4U1E, 3BPJ, 6FEC	6TB3, 6FYX, 4U1E	6TB3, 3BPJ
Non-hydrogen atoms	76,380	78,384	81,866
Protein residues	8,027	7,845	5,612
RNA bases	1,719	1,852	1,771
R.m.s. deviations			
Bond lengths (Å)			0.009
Bond angles (°)			1.245
Validation			
MolProbity score			1.26
Clash score			4.91
Rotamer outliers (%)			0.19
Ramachandran plot			
Favored (%)			99.17
Allowed (%)			0.78
Disallowed (%)			0.05
Validation RNA			
Correct sugar pucker (%)			99
Good backbone conf. (%)			71

Appendix Table S2 - Data collection, refinement, and validation statistics of the human 43S PIC.

Atomic models were built into the best-resolved maps as obtained after local focused refinement or multi-body refinement. Validation statistics are shown for each individual part, as well as for the final composite models. The model for State II includes 40S SSU, eIF1, eIF3 PCI-MPN core, eIF3d, eIF3c-N, eIF3a-C, eIF3b, eIF3i, eIF3j, RRM and ABCE1. The model for State III includes 40S SSU, eIF1, eIF1A, eIF2α/β/γ, $tRNA_i$, eIF3 PCI-MPN core, eIF3d, eIF3c-N, eIF3a-C, eIF3b, eIF3i, RRM and ABCE1.

***H.s.* 43S**	**40S eIF1A eIF3c-N eIF3d**	**eIF3 PCI-MPN core (3a, 3c, 3d-N, 3e, 3f, 3h, 3k, 3l, 3m)**	**Ternary complex (eIF2α/β/γ, $tRNA_i$ eIF1)**	**ABCE1**	**composite model (state II) (PDB 6ZVJ, EMDB 11458)**	**composite model (state III) (PDB 7A09, EMDB 11602)**
Data collection						
Voltage (kV)	300					
Electron exposure (e–/Å^2)	48					
Defocus range (μm)	−0.5 to −2.5					
Pixel size (Å)	1.059					
Symmetry imposed	C1					
Refinement						
Particle images (no.)	23,660	25,228	11,032	13,250	5,231	8,712
Map resolution (Å)	3.0/3.0 (40S body/head)	3.4/3.8 (a,c,d,e,f,h, k,l,m)	4	3.2	3.8	3.5
FSC threshold	0.143					
Map sharpening B factor (Å^2)	-29.98/ -35.86	-61.34/- 89.07	-50.55	-45.58	-36.79	-34.39
Model composition						
Correlation coefficient (%; mask; Phenix)	85/84	81	51	80	69	75
Starting model (PDB codes)	40S: 6G5H eL41: 6EK0 eIF1A: 3J81 eIF3d: 5K4B	5A5T	tRNA: 6FEC eIF2β: 6GSM eIF2α,γ: 6O85 eIF1: 6GSM	5LL6		
Non-hydrogen atoms	50,220/ 27,787	25,291	7,889	4,619	115,031	122,211
Protein residues	3,043/ 2,239	3,104	973	576	10,127	10,954
RNA bases	1208/ 464	0	75	0	1,720	1,796
R.m.s. deviations						
Bond lengths (Å)	0.017/0.024	0.016	0.013	0.017	0.010	0.010
Bond angles (°)	1.425/1.757	1.587	1.578	1.558	1.337	1.203

Validation						
MolProbity score	1.79/2.05	1.5	1.93	2.21	1.4	1.98
Clash score	2.82/4.36	6.52	7.9	6.45	5.45	8.57
Rotamer outliers (%)	8.9/12.64	1.53	3.83	13.44	1.39	0.02
Ramachandran plot						
Favored (%)	99.63/99.18	99.74	97.74	99.48	99.76	90.96
Allowed (%)	0.37/0.77	0.26	1.54	0.52	0.24	8.98
Disallowed (%)	0/0.05	0	0.71	0	0	0.06
Validation RNA						
Correct sugar pucker (%)	99.17/98.71	-	100	-	100	100
Good backbone conf. (%)	73.43/75	-	69.33	-	70	70

Appendix Table S3 - Crosslinks identified on a yeast ABCE1-43S PIC.

ABCE1-bound 43S PIC was affinity-purified from yeast cell extracts using TAP-tagged Nip1 (eIF3c) protein and crosslinked with BS2G. 43 inter-protein (dark green) and 74 intra-protein (light green) crosslinks were obtained from the analysis. The crosslinks are listed according to the Id.Score (xQuest identification score).

No	Topology	Protein1	Protein2	AbsPos1	AbsPos2	Mz	z	Error	Id.Score
1	TLVNKSTGLK-VAKSNR-a5-b3	sp|P33442|RS3A1_YEAST	sp|P26783|RS5_YEAST	50	222	610.686	3	-1.1	42.07
2	NKDDLEKISK-IAKER-a7-b3	sp|P38249|EIF3A_YEAST	sp|P32497|EIF3C_YEAST	596	802	476.015	4	0.1	40.46
3	ALQKEQEEQALK-STALKILAGK-a4-b5	sp|Q05775|EIF3J_YEAST	sp|Q03195|RLI1_YEAST	118	121	628.607	4	0.7	39.23
4	TGPKALPDAVTIIEPK-VKQLENVSSNIVK-a4-b2	sp|P05750|RS3_YEAST	sp|P38701|RS20_YEAST	200	32	801.455	4	1.2	39.09
5	DDLEKISK-IAKER-a5-b3	sp|P38249|EIF3A_YEAST	sp|P32497|EIF3C_YEAST	596	802	553.637	3	-0.9	37.91
6	ENKVSPADAAK-VIKVLGR-a3-b3	sp|P39938|RS26A_YEAST	sp|Q3E7X9|RS28A_YEAST	108	14	503.041	4	0.5	37.53
7	GISFKLQEEERER-SFKEPR-a5-b3	sp|P02407|RS17A_YEAST	sp|P32905|RSSA1_YEAST	72	116	496.658	5	-0.3	35.5
8	DSATHELTKVSEEPIHK-VHKSVAER-a9-b3	sp|P40217|EIF3I_YEAST	sp|Q04067|EIF3G_YEAST	138	47	589.106	5	-1.4	34.7
9	GISFKLQEEER-SFKEPR-a5-b3	sp|P02407|RS17A_YEAST	sp|P32905|RSSA1_YEAST	72	116	732.043	3	0.1	34.7
10	NKSELESR-IQKEK-a2-b3	sp|P38249|EIF3A_YEAST	sp|Q04067|EIF3G_YEAST	709	97	568.305	3	1.2	34.63
11	ISKIVDER-IAKER-a3-b3	sp|P38249|EIF3A_YEAST	sp|P32497|EIF3C_YEAST	599	802	557.653	3	-1	34.28
12	EKVEEQEQQQQQIIK-VTPTKTEVIIR-a2-b5	sp|P38701|RS20_YEAST	sp|P05750|RS3_YEAST	8	45	809.941	4	1.1	34.14
13	ANDIGFHKYR-ITLTSTKVK-a8-b7	sp|P41058|RS29B_YEAST	sp|P38701|RS20_YEAST	54	30	577.319	4	1.3	33.77
14	QTVATLNVLIKDK-AGKVK-a11-b3	sp|Q05775|EIF3J_YEAST	sp|P0CX33|RS30A_YEAST	205	13	510.808	4	1.1	33.54
15	ALQKEQEEQALK-AIKGPVQK-a4-b3	sp|Q05775|EIF3J_YEAST	sp|Q03195|RLI1_YEAST	118	181	588.331	4	0.8	31.95
16	LTGDDQKFGVPVR-KAFTSYDR-a7-b1	sp|P38011|GBLP_YEAST	sp|P0CX51|RS16A_YEAST	53	107	629.322	4	0.5	31.91
17	LAAPENEKPAPVRTHMR-EKAKR-a8-b4	sp|Q01855|RS15_YEAST	sp|P39730|IF2P_YEAST	72	226	881.813	3	3.2	31.89

18	KVQLGK-VEKASR-a1-b3	sp|P0CX35|RS4A_YEAST	sp|P0CX31|RS24A_YEAST	128	102	364.968	4	-0.7	31.84
19	EFIILGGGQEAKDVTTTSANEGK-HKVEHGYK-a12-b2	sp|P40217|EIF3I_YEAST	sp|P06103|EIF3B_YEAST	261	632	865.188	4	1.2	31.73
20	AVLKFAAHTGATPIAGR-KDQYVPEVSALDLSR-a4-b1	sp|P32905|RSSA1_YEAST	sp|P02407|RS17A_YEAST	88	81	699.979	5	0.7	31.21
21	LVEGLANDPENKVPLIK-VDAEGKVTK-a12-b6	sp|P48589|RS12_YEAST	sp|P05759|RS31_YEAST	85	113	723.401	4	0.5	31.13
22	AAKAAAALAGGK-NTKGGK-a3-b3	sp|Q3E792|RS25A_YEAST	sp|P38912|IF1A_YEAST	12	7	566.988	3	-1.1	30.51
23	NKSELESR-EKASLTK-a2-b2	sp|P38249|EIF3A_YEAST	sp|Q04067|EIF3G_YEAST	709	99	611.991	3	0.6	30.48
24	AAAALAGGKK-KKDELER-a9-b1	sp|Q3E792|RS25A_YEAST	sp|P26783|RS5_YEAST	21	213	468.265	4	-1.3	30.06
25	TGPKALPDAVTIIEPKEEEPILAPSVK-VKQLENVSSNIVK-a4-b2	sp|P05750|RS3_YEAST	sp|P38701|RS20_YEAST	200	32	879.894	5	2.3	29.65
26	YIDLEAPVQIVKR-VTPTKTEVIIR-a12-b5	sp|P38701|RS20_YEAST	sp|P05750|RS3_YEAST	101	45	724.67	4	0.7	29.58
27	DVTTTSANEGKFEAR-EKASLTK-a11-b2	sp|P40217|EIF3I_YEAST	sp|Q04067|EIF3G_YEAST	272	99	833.087	3	0.9	29.21
28	REDDKPK-EKAKR-a5-b4	sp|P39935|IF4F1_YEAST	sp|P39730|IF2P_YEAST	564	226	538.627	3	2.7	29
29	GGTATGGAGKK-VEASCFDGNKR-a10-b10	sp|Q05775|EIF3J_YEAST	sp|P38912|IF1A_YEAST	230	56	761.367	3	0.6	28.42
30	AAAEKSQKSK-KMKSLLNK-a8-b3	sp|P39730|IF2P_YEAST	sp|P39935|IF4F1_YEAST	147	611	702.066	3	0.7	28.2
31	AAAEKSQKSK-KMKSLLNK-a8-b3	sp|P39730|IF2P_YEAST	sp|P39936|IF4F2_YEAST	147	571	702.066	3	0.7	28.2
32	QVIIAEVSKNK-IQKEK-a9-b3	sp|P38249|EIF3A_YEAST	sp|Q04067|EIF3G_YEAST	707	97	493.039	4	0	28.19
33	AIKLTGHERPLTQVK-SIITYKIEDGVK-a3-b6	sp|P40217|EIF3I_YEAST	sp|Q04067|EIF3G_YEAST	5	23	631.161	5	-0.2	27.51
34	KAATASANVR-NKAVAR-a1-b2	sp|P38431|IF5_YEAST	sp|P32497|EIF3C_YEAST	156	189	581.326	3	-2.5	26.73
35	AEGKLLTRK-KAALEKK-a4-b1	sp|P39730|IF2P_YEAST	sp|P39935|IF4F1_YEAST	235	217	633.386	3	-0.1	26.42
36	AQHAVILDQEKYDR-IVYALTTIKGVGR-a11-b9	sp|Q3E792|RS25A_YEAST	sp|P0CX55|RS18A_YEAST	46	36	793.683	4	-2.1	26.14
37	AGNREPPSTPSTLPKATVSPDK-KNGLISETEK-a15-b1	sp|P38249|EIF3A_YEAST	sp|P39936|IF4F2_YEAST	889	243	693.563	5	-2	25.49
38	QNDITDGKDYHTLANNVESK-VFKTHSYR-a8-b3	sp|P0CX55|RS18A_YEAST	sp|Q01855|RS15_YEAST	96	13	679.733	5	1.5	25.1
39	IAIVSADKCKPK-EDDKPK-a10-b4	sp|Q03195|RLI1_YEAST	sp|P39935|IF4F1_YEAST	17	564	539.787	4	-1.9	24.77
40	VSVVRNKETGK-LANEEKMK-a7-b6	sp|Q04067|EIF3G_YEAST	sp|P39730|IF2P_YEAST	227	210	569.308	4	-1	23.08
41	DVAKPMSIESIR-KKAATASANVR-a4-b2	sp|Q05775|EIF3J_YEAST	sp|P38431|IF5_YEAST	186	156	640.102	4	2.2	22.92
42	DVLDELKNYISKR-EIVKSNTSSKK-a7-b4	sp|P20459|IF2A_YEAST	sp|P39015|STM1_YEAST	170	27	485.598	6	-4	22.73
43	YGLAEKVEK-DCKACGK-a6-b3	sp|P0CX31|RS24A_YEAST	sp|P38431|IF5_YEAST	99	122	657.319	3	2.6	22.61
44	VGELLKLR-SPEDVKR-a6-b6	sp|Q03195|RLI1_YEAST	sp|Q03195|RLI1_YEAST	192	203	464.018	4	-0.9	43.08
45	ILQLENVLKR-VGELLKLR-a9-b6	sp|Q03195|RLI1_YEAST	sp|Q03195|RLI1_YEAST	216	192	562.85	4	0.4	42.5
46	FNVVKVSAAAGK-NAGLGFKTPK-a5-b7	sp|P0CX48|RS11B_YEAST	sp|P0CX48|RS11B_YEAST	141	43	580.329	4	1.8	41.37
47	NTEEKGWVPVTK-LVKAGK-a5-b3	sp|P25443|RS2_YEAST	sp|P25443|RS2_YEAST	33	46	700.057	3	1	41.06
48	AQHAVILDQEKYDR-LKIGGSLAR-a11-b2	sp|Q3E792|RS25A_YEAST	sp|Q3E792|RS25A_YEAST	46	70	539.897	5	0.5	40.72

49	GPVQKVGELLK-ILQLENVLKR-a5-b9	sp|Q03195|RLI1_YEAST	sp|Q03195|RLI1_YEAST	186	216	622.878	4	1.4	39.24
50	SDWLLLKK-SIDTLKDK-a7-b6	sp|P39730|IF2P_YEAST	sp|P39730|IF2P_YEAST	993	976	505.037	4	0.7	38.85
51	AQHAVILDQEKYDR-AAAALAGGKK-a11-b9	sp|Q3E792|RS25A_YEAST	sp|Q3E792|RS25A_YEAST	46	21	528.486	5	0.4	38.73
52	EKVEEQEQQQQQIIK-YIDLEAPVQIVKR-a2-b12	sp|P38701|RS20_YEAST	sp|P38701|RS20_YEAST	8	101	881.722	4	0.5	38.37
53	ASLTKTGLQCR-IQKEK-a5-b3	sp|Q04067|EIF3G_YEAST	sp|Q04067|EIF3G_YEAST	104	97	659.027	3	0.9	38.32
54	ALTSLFSKAGK-SFHGKR-a8-b5	sp|P06103|EIF3B_YEAST	sp|P06103|EIF3B_YEAST	105	147	488.021	4	-1.2	38.05
55	LSSESVIEQIVKYAR-KGLTPSQIGVLLR-a12-b1	sp|P05756|RS13_YEAST	sp|P05756|RS13_YEAST	39	43	800.459	4	0.6	37.83
56	RKEEIANAER-LAKGGR-a2-b3	sp|P38249|EIF3A_YEAST	sp|P38249|EIF3A_YEAST	835	961	478.765	4	-0.6	37.72
57	VQTKLTR-ELEKK-a4-b4	sp|P26786|RS7A_YEAST	sp|P26786|RS7A_YEAST	76	83	529.642	3	-0.9	37.4
58	KLDYVLALK-VGVLSEDKK-a1-b8	sp|P05755|RS9B_YEAST	sp|P05755|RS9B_YEAST	92	90	533.811	4	0	37.27
59	ALQKEQEEQALK-KGKESSADR-a4-b3	sp|Q05775|EIF3J_YEAST	sp|Q05775|EIF3J_YEAST	118	62	622.573	4	-0.2	37.1
60	ILQLENVLKR-SPEDVKR-a9-b6	sp|Q03195|RLI1_YEAST	sp|Q03195|RLI1_YEAST	216	203	538.56	4	0.6	37.08
61	APFVVALNKIDR-TKLLDK-a9-b2	sp|P39730|IF2P_YEAST	sp|P39730|IF2P_YEAST	531	420	539.568	4	0	36.93
62	DIEKLSGGELQR-ILQLENVLKR-a4-b9	sp|Q03195|RLI1_YEAST	sp|Q03195|RLI1_YEAST	221	216	889.17	3	2.3	36.86
63	KAPFVVALNKIDR-TKLLDK-a10-b2	sp|P39730|IF2P_YEAST	sp|P39730|IF2P_YEAST	531	420	571.592	4	0.4	36.58
64	LNNVFVIGEQGKPYISLPK-VNDTVKIDLASGK-a12-b6	sp|P0CX35|RS4A_YEAST	sp|P0CX35|RS4A_YEAST	233	161	893.492	4	0.8	36.39
65	VCEFMISQLGLQKK-NIKIHGF-a13-b3	sp|P32911|SUI1_YEAST	sp|P32911|SUI1_YEAST	100	104	651.848	4	-0.2	36.2
66	AQHAVILDQEKYDR-AAKAAAALAGGK-a11-b3	sp|Q3E792|RS25A_YEAST	sp|Q3E792|RS25A_YEAST	46	12	556.9	5	-0.5	36.03
67	YGSEKGSPAGPSAVTAR-IEDGVKYK-a5-b6	sp|Q04067|EIF3G_YEAST	sp|Q04067|EIF3G_YEAST	62	29	671.092	4	0.5	35.94
68	ALQKEQEEQALK-GKESSADR-a4-b2	sp|Q05775|EIF3J_YEAST	sp|Q05775|EIF3J_YEAST	118	62	590.549	4	-0.9	35.75
69	AQHAVILDQEKYDR-ILKEVPTYR-a11-b3	sp|Q3E792|RS25A_YEAST	sp|Q3E792|RS25A_YEAST	46	52	580.711	5	-1.9	35.63
70	KAATASANVR-DCKACGK-a1-b3	sp|P38431|IF5_YEAST	sp|P38431|IF5_YEAST	156	122	641.312	3	-1.3	35.61
71	YGSEKGSPAGPSAVTAR-VHKSVAER-a5-b3	sp|Q04067|EIF3G_YEAST	sp|Q04067|EIF3G_YEAST	62	47	664.594	4	1.8	35.58
72	NVKEEETVAK-SKNAER-a3-b2	sp|P0CX39|RS8A_YEAST	sp|P0CX39|RS8A_YEAST	128	137	649.332	3	-0.9	35.57
73	FYAPETKEK-TDVIKR-a7-b5	sp|P06103|EIF3B_YEAST	sp|P06103|EIF3B_YEAST	529	536	647.011	3	0	35.56
74	DIEKLSGGELQR-GPVQKVGELLK-a4-b5	sp|Q03195|RLI1_YEAST	sp|Q03195|RLI1_YEAST	221	186	869.818	3	1.3	35.54
75	ALLDIDTLDEKTR-GKESSADR-a11-b2	sp|Q05775|EIF3J_YEAST	sp|Q05775|EIF3J_YEAST	79	62	612.562	4	0	35.39
76	AAKLAAPENEKPAPVR-VFKTHSYR-a3-b3	sp|Q01855|RS15_YEAST	sp|Q01855|RS15_YEAST	64	13	466.589	6	-1.7	35.26
77	TGPKALPDAVTIIEPK-DPAKSR-a4-b4	sp|P05750|RS3_YEAST	sp|P05750|RS3_YEAST	200	194	605.336	4	-2.1	34.52
78	ALQKEQEEQALK-KEQPKK-a4-b5	sp|Q05775|EIF3J_YEAST	sp|Q05775|EIF3J_YEAST	118	56	567.563	4	1.1	34.31
79	GGTATGGAGKK-GKTNLGGAFK-a10-b2	sp|Q05775|EIF3J_YEAST	sp|Q05775|EIF3J_YEAST	230	236	664.688	3	-1.7	34.19

80	TTQENASEAIKSDSK-KDSEVVPDDELK-a11-b1	sp|P39730|IF2P_YEAST	sp|P39730|IF2P_YEAST	298	303	770.123	4	1.1	34.13
81	ASLTKTGLQCR-NKETGK-a5-b2	sp|Q04067|EIF3G_YEAST	sp|Q04067|EIF3G_YEAST	104	227	669.351	3	1.1	34.09
82	ALQKEQEEQALK-ELIKK-a4-b4	sp|Q05775|EIF3J_YEAST	sp|Q05775|EIF3J_YEAST	118	86	714.067	3	-0.2	33.94
83	YIDLEAPVQIVKR-VLKISTR-a12-b3	sp|P38701|RS20_YEAST	sp|P38701|RS20_YEAST	101	64	614.614	4	1	33.77
84	KQFVVDVLHPNR-LAEVYKAEK-a1-b6	sp|P0CX31|RS24A_YEAST	sp|P0CX31|RS24A_YEAST	21	49	650.107	4	-1	33.63
85	RPAFTKDTPIETHPLFNAETK-ALQKEQEEQALK-a6-b4	sp|Q05775|EIF3J_YEAST	sp|Q05775|EIF3J_YEAST	132	118	654.677	6	0.9	33.38
86	ALLDIDTLDEKTRK-ELIKK-a11-b4	sp|Q05775|EIF3J_YEAST	sp|Q05775|EIF3J_YEAST	79	86	786.117	3	0.3	33.35
87	ATVSPDKAK-LDMIAQKQR-a7-b7	sp|P38249|EIF3A_YEAST	sp|P38249|EIF3A_YEAST	896	905	529.288	4	0.7	33.28
88	AQHAVILDQEKYDR-SMKDR-a11-b3	sp|Q3E792|RS25A_YEAST	sp|Q3E792|RS25A_YEAST	46	33	605.053	4	-0.4	32.77
89	GKESSADR-ELIKK-a2-b4	sp|Q05775|EIF3J_YEAST	sp|Q05775|EIF3J_YEAST	62	86	525.618	3	0.4	32.67
90	SLEHYDKLSFQGPPETLR-LNKEYK-a7-b3	sp|P32497|EIF3C_YEAST	sp|P32497|EIF3C_YEAST	661	796	752.386	4	-0.9	32.18
91	NPPDSVSGSKK-KAATASANVR-a10-b1	sp|P38431|IF5_YEAST	sp|P38431|IF5_YEAST	152	156	550.54	4	-0.3	31.91
92	EKVEEQEQQQQQIIK-VLKISTR-a2-b3	sp|P38701|RS20_YEAST	sp|P38701|RS20_YEAST	8	64	699.884	4	0	31.42
93	MITEVNAKGHVYIDPNEAK-NKSELESR-a8-b2	sp|P38249|EIF3A_YEAST	sp|P38249|EIF3A_YEAST	679	709	797.399	4	0.1	31.28
94	ALQKEQEEQALK-KPAPKPK-a4-b5	sp|Q05775|EIF3J_YEAST	sp|Q05775|EIF3J_YEAST	118	49	569.573	4	0.4	31.24
95	EQEEQALKRPAFTK-ALQKEQEEQALK-a8-b4	sp|Q05775|EIF3J_YEAST	sp|Q05775|EIF3J_YEAST	126	118	637.737	5	0.8	30.87
96	YGSEKGSPAGPSAVTAR-ITQKVK-a5-b4	sp|Q04067|EIF3G_YEAST	sp|Q04067|EIF3G_YEAST	62	35	612.331	4	1.8	30.64
97	VDEVQGKNLLTNFHGMDFTTDK-TLVNKSTGLK-a7-b5	sp|P33442|RS3A1_YEAST	sp|P33442|RS3A1_YEAST	94	50	916.969	4	-0.5	30.62
98	DTPIETHPLFNAETKR-GKESSADR-a15-b2	sp|Q05775|EIF3J_YEAST	sp|Q05775|EIF3J_YEAST	147	62	704.099	4	0.7	30.5
99	LRVDEVQGKNLLTNFHGMDFTTDK-TLVNKSTGLK-a9-b5	sp|P33442|RS3A1_YEAST	sp|P33442|RS3A1_YEAST	94	50	787.612	5	-2.7	30.1
100	GFLFVECGSMNDAKK-IIKSFHGK-a14-b3	sp|P06103|EIF3B_YEAST	sp|P06103|EIF3B_YEAST	138	142	682.596	4	-1.7	29.94
101	LKVVFGIE-SIDTLKDK-a2-b6	sp|P39730|IF2P_YEAST	sp|P39730|IF2P_YEAST	996	976	640.363	3	-0.1	29.77
102	DTPIETHPLFNAETKR-ALQKEQEEQALK-a15-b4	sp|Q05775|EIF3J_YEAST	sp|Q05775|EIF3J_YEAST	147	118	845.435	4	-0.8	29.56
103	AGNREPPSTPSTLPKATVSPDK-AKLDMIAQK-a15-b2	sp|P38249|EIF3A_YEAST	sp|P38249|EIF3A_YEAST	889	898	673.359	5	0	29.43
104	DLSEASVYPEYALPKTYNK-ENKVSPADAAK-a15-b3	sp|P39938|RS26A_YEAST	sp|P39938|RS26A_YEAST	66	108	853.926	4	0.2	29.34
105	ALQKEQEEQALK-TRKELIK-a4-b3	sp|Q05775|EIF3J_YEAST	sp|Q05775|EIF3J_YEAST	118	82	480.273	5	-0.1	29.06
106	AGNREPPSTPSTLPKATVSPDK-KSTPYSFR-a15-b1	sp|P38249|EIF3A_YEAST	sp|P38249|EIF3A_YEAST	889	867	666.946	5	0.9	28.39
107	AQHAVILDQEKYDR-HSKQAIYTR-a11-b3	sp|Q3E792|RS25A_YEAST	sp|Q3E792|RS25A_YEAST	46	97	577.7	5	-0.9	28.21
108	EPPSTPSTLPKATVSPDK-KSTPYSFR-a11-b1	sp|P38249|EIF3A_YEAST	sp|P38249|EIF3A_YEAST	889	867	733.879	4	-0.7	25.78
109	EQEEQALKRPAFTK-KEQPK-a8-b1	sp|Q05775|EIF3J_YEAST	sp|Q05775|EIF3J_YEAST	126	52	600.568	4	-2.8	25.66
110	AASAKIESSVESQFSAGR-NVKEEETVAK-a5-b3	sp|P0CX39|RS8A_YEAST	sp|P0CX39|RS8A_YEAST	151	128	767.388	4	1.4	25.61

111	VVAQVEDAVNNTQQADLKNK-NKAVARAYNTTK-a18-b2	sp|P32497|EIF3C_YEAST	sp|P32497|EIF3C_YEAST	187	189	904.724	4	0.4	25.46
112	VTGFKDEVLETV-TLVNKSTGLK-a5-b5	sp|P33442|RS3A1_YEAST	sp|P33442|RS3A1_YEAST	248	50	831.456	3	1.3	25.42
113	QNDITDGKDYHTLANNVESK-KADVDLHKR-a8-b1	sp|P0CX55|RS18A_YEAST	sp|P0CX55|RS18A_YEAST	96	49	688.544	5	0.6	24.42
114	ALQKEQEEQALK-GGTATGGAGKK-a4-b10	sp|Q05775|EIF3J_YEAST	sp|Q05775|EIF3J_YEAST	118	230	604.317	4	-2.8	24.37
115	EPPSTPSTLPKATVSPDK-AKLDMIAQK-a11-b2	sp|P38249|EIF3A_YEAST	sp|P38249|EIF3A_YEAST	889	898	741.895	4	-1.3	24.37
116	KADVPPPSADPSK-EIVKSNTSSK-a1-b4	sp|P39015|STM1_YEAST	sp|P39015|STM1_YEAST	34	27	832.765	3	-1.2	23.52
117	ALTAAITPMNKK-GGTATGGAGKK-a11-b10	sp|Q05775|EIF3J_YEAST	sp|Q05775|EIF3J_YEAST	166	230	565.311	4	0.7	22.52

Appendix Table S4 - Molecular interactions between eIF3 subunits and 40S.

eIF3a									
3a	**eS1**	3a	**3c**	3a	**3f**	3a	**3h**	3a	**3m**
Q6	E78	E125	K474	N521	S232	N521	S232	S444	K342
N10	E78	V132	N678	H565	R109	A525	Q314	I446	I325
R14	E78, D77	R140	P464,S466			E547	K220	Y447	K342
E17	N75	R143	D463			H550	W216	Q448	I325
		W246	P729			E564	H209	S449	D326, Q327
		Q247	Q724			R571	E77	E451	Q327
		D337	K745			E576	R108	R454	E309
		L342	R719			R578	E145, E146	N512	C323
		E468	Y799						
		R483	S797, D800						
		I484	D800						

eIF3b			
3b	**18S rRNA**	3b	**uS4**
K487	A560	R507	D158
D488	A560	V556	K155

3c-N		eIF3c (PCI-MPN core)											
3c	**18S rRNA**	3c	**18S rRNA**	3c	**eS27**	3c	**3d**	3c	**3e**	3c	**3f**	3c	**3h**
R47	C1039, A1181	K342	G929	G341	Q65	D562	A70	Y583	Y286	Q852	D333	Y557	L210
K55	C1180	K343	G929	N388	Q75	M591	Q31	D587	Y286	N870	N351, Q347	L859	M247
K92	U1178			L389	Q75	H593	P32, G64	D602	Y41			K862	M247
K132	C369					Q595	L39	S820	N302			V873	N261
K136	U367					H600	H73	L835	I347, Q349			H876	N261
Q143	U367, U368					D602	H73	Q837	S352				
K144	U367					P603	W45	H845	N395				
						Q606	W45						
						Y609	K41						
						N610	A43						
						N631	R38						
						D635	Y59						
						R641	T46						
						E666	W45						

eIF3d									
3d	**3e**	3d	**uS27**	3d	**18S rRNA**	3d	**eS28**	3d	**uS7**
F4	Y32	E75	K36	R212	C1470	Q416	R51, E52	K472	Q29
Q10	H12	E77	R80			T423	R13	S478	N31
D11	R16	Q81	S78, F79			K426	F34, T38		
W16	S167, G171	V83	G76						
G17	W170								
A20	Q209								
Y30	L208								
F33	N244, L590								
K35	Q283, E284								

eIF3e	
3e	**3l**
R369	D480
Y401	I523
Q416	D532

eIF3f							
3f	**3h**	3f	**3k**	3f	**3m**	3f	**3l**
R108	D113	S267	Q218	Q280	N362	N332	I523
V163	Y99	N328	E203	D301	W347		
S164	E56			R306	H339		
Y239	L218, E217			N313	S337		
N260	K206						
R261	H209, N207						
I263	I205						
D268	Q336						
Q271	S161						
P316	Q348						
I318	Q348						
N342	K331						
Q345	N324						
N356	R313						

eIF3h			
3h	**3l**	3h	**3k**
E195	R545	K331	S217
		K345	K204

eIF3l	
3l	**3k**
K534	S216

Appendix text 1 - Molecular interactions between eIF3j and the 40S subunit in the yeast 43S-PIC.

Molecular details of the eIF3j-40S interaction were derived from the high-resolution structure of the cross-linked 43S-PIC (43S-PIC-XL) at an overall resolution of 3.0 Å and a local resolution of eIF3j ranging from 3 to 5 Å (Appendix Fig S4). Ribosome-bound eIF3j forms a dimer folding into a stable entangled 6-helix bundle as observed in crystal structure of human eIF3j (PDB 3BPJ; lacking 137 residues at the N- and 28 residues at the C-terminus). A yeast homology model based on this structure could be unambiguously fitted into the EM density (Fig EV3). It accommodates between the 40S body and head *via* interactions of both protomers. The 40S body is contacted by Arg148 and Arg154 of the N-terminal helix 1 of protomer 1 *via* A542 in the h17-h18 junction and *via* Glu22 of eS30, respectively. This contact to eS30 is also confirmed by the XL-MS data (Appendix Fig S5 and Appendix Table 3). 40S body and head are bridged by the C-terminal helix 3 of protomer 1. Here, Gln195 and Thr199 contact the backbone of eS30 in the body (at Lys15 and Lys20, respectively), while Arg215 contacts G1264 of h33 on the head. Helix 3 of the second protomer projects into the opposite direction and likely contacts Glu31 of eIF1A *via* a basic patch consisting of Lys205, Arg209, and Arg212. Following helix 3, the second eIF3j protomer forms a highly basic loop inside a pocket formed by h33, h34 and eS10 (Figs 4E, F and EV3). Here, Lys230 of eIF3j and Phe59 of eS10 are sandwiching the flipped-out G1435 base of h34. H34 is also contacted by Lys234 (at G1438), whereas Lys231 contacts U1266 and G1267 of h33. The loop is further stabilized by salt bridges between Arg220 and Glu70-Glu71 of eS10. From the loop, the C-terminus projects towards the mRNA entry channel (Fig 4G). It interacts with h18 (*via* Lys236) and then forms several contacts with uS3, mainly *via* hydrophobic interactions between Leu239 and Phe243 with Ile114, Leu142, and Arg143 of uS3 and the flipped-out base of A579 (h18). Finally, the C-terminus is anchored at h18 by the interaction of Lys244 with C559 (phosphate) and U581 (stacking), as well as Lys245 with U581 and U582 (phosphates). From here, the eIF3j C-terminus makes another kink into the mRNA entry channel, in which eleven more residues are visible (Asp246-Phe257). This part is not forming any specific interactions and thus is more flexible.

Appendix References

des Georges A, Dhote V, Kuhn L, Hellen CU, Pestova TV, Frank J, Hashem Y (2015) Structure of mammalian eIF3 in the context of the 43S preinitiation complex. Nature 525: 491-495

Erzberger JP, Stengel F, Pellarin R, Zhang S, Schaefer T, Aylett CHS, Cimermancic P, Boehringer D, Sali A, Aebersold R et al (2014) Molecular Architecture of the 40SeIF1eIF3 Translation Initiation Complex. Cell 159: 1227-1228

Liu Y, Neumann P, Kuhle B, Monecke T, Schell S, Chari A, Ficner R (2014) Translation initiation factor eIF3b contains a nine-bladed beta-propeller and interacts with the 40S ribosomal subunit. Structure 22: 923-930

Llacer JL, Hussain T, Saini AK, Nanda JS, Kaur S, Gordiyenko Y, Kumar R, Hinnebusch AG, Lorsch JR, Ramakrishnan V (2018) Translational initiation factor eIF5 replaces eIF1 on the 40S ribosomal subunit to promote start-codon recognition. Elife 7